Published in final edited form as:
ACS Nano. 2011 October 25; 5(10): 8013–8018. doi:10.1021/nn2024896.

Aqueous, Protein-Driven Synthesis of Transition Metal-Doped ZnS Immuno-Quantum Dots

Weibin Zhou and **François Baneyx***
Department of Chemical Engineering, University of Washington, Box 351750, Seattle, WA 98195

Abstract

The intentional introduction of transition metal impurities in semiconductor nanocrystals is an attractive approach for tuning quantum dot (QD) emission over a wide range of wavelengths. However, the development of effective doping strategies can be challenging, especially if one simultaneously requires a low toxicity crystalline core, a functional protein shell, and a “green”, single-step synthesis process. Here, we describe a simple and environmentally friendly route for the biofabrication of Cu-doped (blue-green) or Mn-doped (yellow-orange) ZnS nanocrystals surrounded by an antibody-binding protein shell. The ZnS:Mn hybrid particles obtained with this method exhibited a 60% enhancement in maximum photoluminescence intensity relative to undoped nanocrystals and have a hydrodynamic diameter inferior to 10 nm. They can be stored for months at 4°C, are stable over a physiological range of pH and salt concentrations, can be decorated with variable amounts of antibodies by direct mixing, and hold promise for biosensing and imaging applications.

Keywords

Quantum dot; Imaging; Molecular Biomimetics; Bionanotechnology

Semiconductor nanocrystals or quantum dots (QDs) are an attractive alternative to organic dyes due to their brightness, photostability, large Stokes’ shifts, and the possibility of tuning emission wavelength maxima by altering the size or composition of the crystalline core.[1–5] They have been made from IV, III-V and II-VI semiconductors, and are typically synthesized *via* thermal decomposition of organometallic precursors in organic solvents and in the presence of surfactants.[6] The most popular QDs consists of a CdSe core surrounded by a ZnS shell that is itself capped by a hydrophobic ligand (often trioctylphosphine oxide; TOPO).[7,8] For biological applications, such QDs must be made hydrophilic by ligand exchange and further derivatized with antibodies or other targeting molecules.[4] While this synthesis train works well, it is energy intensive, involves toxic compounds, greatly increases the size of the particle, and relies on a series of cumbersome and time-consuming steps.

Molecular biomimetics is a “green” approach to material synthesis in which short peptides selected by combinatorial display for their ability to bind inorganic materials[9] are used in isolation or within the context or larger proteins, to synthesize or assemble structures with nanoscale control of composition and architecture.[10–12] Previously, we described the construction, overproduction and rapid purification of a fusion protein combining ZnS-mineralizing and antibody-binding activities and demonstrated that it could be used for the efficient and environmentally friendly biosynthesis of ZnS nanocrystals emitting in the blue

Address correspondence to: baneyx@uw.edu.

region of the spectrum.[13] By taking advantage of the functional protein shell, these nanoparticles could be decorated with antibodies in a single, aqueous reaction pot, yielding immuno-QDs that, at ≈ 14 nm in hydrodynamic diameter (HD), are significantly smaller than those generated by mixing streptavidin-coated QDs (HD ≈ 25–35 nm)[14] with biotinylated antibodies (HD ≈ 10 nm).[13] Because different emission wavelengths are desirable for QD-based imaging and multiplexing technologies,[2–5] we explore here the possibility of altering alter the photoluminescence color of the ZnS core by transition metal doping[15–18] during the biofabrication process. We show that both Cu^{2+} and Mn^{2+} are appropriate dopants and that ZnS:Mn core QDs are bright, stable, derivatizable with variable numbers of antibodies, and useful for practical applications.

RESULTS AND DISCUSSION

Previously, we described a tripartite fusion protein consisting of a ZnS-binding peptide engineered within the active site loop of *Escherichia coli* Thioredoxin 1 (TrxA) fused to the BB antibody-binding module of *Staphylococcus aureus* protein A.[13] In aqueous solvents and under ambient conditions, this designer protein (BB-TrxA::CT43; Fig. 1A) templates the mineralization of luminescent ZnS nanocrystals that have a quantum yield of 2.5% and appear blue to the eye as a result of contributions from the ZnS band-edge (at 320–340 nm), protein tryptophans (at 345 nm) and trap states at 430–450 nm that are presumably associated with sulfur vacancies in the ZnS lattice (Fig. 1B and D, None).

To determine if the emission color could be altered by manganese doping, we conducted biomineralization experiments with 2 μM BB-TrxA::CT43 and 0.4 mM of Na_2S as described,[13] except that various amounts of $Mn(CH_3COO)_2$ were added to the $Zn(CH_3COO)_2$ electrolyte, keeping the total cation concentration (Zn^{2+} plus Mn^{2+}) equal to 0.4 mM (see Materials and Methods). Compared to control reactions performed in the absence of protein and for which no photoluminescent material is obtained (Fig. 1B, Control), and compared to the blue color of undoped QDs (Fig. 1B, None), a yellow-orange emission characteristic of Mn-doped ZnS became obvious in the presence of 0.5% Mn^{2+}. The emission peak did not shift but increased in intensity with the doping ratio, reaching a maximum at 10% Mn^{2+} and decreasing at higher concentrations (Fig. 1B–C and Fig. S1 in Supporting Information). These doping ratios are significantly higher than the 0.5 to 1% Mn^{2+} values that have been reported to yield maximum photoluminescence in traditional synthesis schemes.[15,19] To determine the extent of manganese incorporation, QDs biofabricated at nominal doping ratios of 7.5% and 10% Mn^{2+} were acetone-precipitated and the concentrations of Mn and Zn determined by induction coupled plasma (ICP) atomic emission spectroscopy. The calculated ratios of maganese to manganese plus zinc were 7.27% and 9.74%, respectively, indicating that the composition of the doped material mirrors the solution chemistry. Why those higher amounts of Mn are required to achieve high photoluminescence remains unclear at present but could be an idiosyncrasy of the protein-aided synthesis process.

QDs biofabricated in the presence of 7.5% Mn^{2+} were selected for detailed characterization. As expected for quantum-confined particles, the absorption edge of ZnS:Mn QDs (~335 nm; Fig. 1D) was blue-shifted relative to bulk ZnS (340 nm for the zinc blende structure), but less so than in the case of undoped nanocrystals (~317 nm). High-resolution TEM imaging confirmed the presence of roughly spherical nanocrystals (Fig. 1D, inset) that were 4.1 ± 0.7 nm in diameter based on 67 particles, a value comparable to that of undoped QDs (4.3 ± 1.1 nm).[13] Emission spectra (Fig. 1E) revealed that Mn-doping resulted in complete disappearance of the trap state at 430 nm to the profit of a narrow emission peak centered at 590 nm. This is fully consistent with incorporation of Mn into the ZnS lattice, and energy transfer from ZnS states to the $^4T_1 \rightarrow {}^6A_1$ Mn^{2+} transition.[18] With a 60% increase in

maximum emission intensity, ZnS:Mn particles were also significantly brighter than their undoped counterparts. Finally, dynamic light scattering measurements revealed that the particles' HD was 9.2 ± 1.0 nm, a value consistent with the presence of an about 2.5 nm thick protein shell surrounding the crystalline core.

ZnS:Mn QDs were physically and optically stable for months when stored at 4°C in synthesis buffer. To determine how variations in ionic strength and pH would affect their stability, freshly biofabricated QDs were treated with NaCl, HCl or NaOH and photoluminescence emission spectra were recorded after 1h incubation at room temperature. Although 150 mM NaCl caused a 20% decrease in peak emission intensity, there was no further degradation of optical properties over time or in the presence of 0.5M NaCl (Fig. 2). Furthermore, the QDs remained as bright as the control at pH ≥ 6 and only under highly alkaline conditions (pH 11) was there a small decrease in peak emission intensity. On the other hand, acidic conditions (pH ≤ 5) led to complete loss of luminescence, presumably due to acid unfolding of the protein shell and dissolution of the ZnS core. Overall, these data indicate that the ZnS:Mn particles are suitable for biological applications.

In addition to Mn, other transition metals can be used to create intermediate energy states below the excitonic states of ZnS nanocrystals, thus changing the photophysical relaxation process.[16] To determine if our protein-aided QD synthesis process was compatible with other dopants, we repeated mineralization experiments in the presence of copper (II) ions. Among the various concentrations tested (Fig. S2), addition of 2.5% Cu^{2+} (as a percent of total Zn^{2+} + Cu^{2+}) led to the brightest blue-green luminescence upon UV excitation (Fig. 3B, inset). As in the case of manganese, copper doping led to quenching of the 430 nm trap state and to the appearance of a new peak at 480 nm (Fig. 3) that likely corresponds to the transition from the ZnS defect level to the copper t_2 level.[20]

An attractive feature of our bio-inspired synthesis process is that it yields high-quality nanocrystals capped with a functional protein shell in a single step. In the current design, the BB domain of the fusion protein should mediate direct conjugation of the QDs to the Fc fragment of immunoglobulin G (IgG) antibodies (Fig. 4A). To verify this functionality, we exploited the fact that ZnS:Mn QDs and human IgG localize at two distinct positions when subjected to electrophoresis on agarose gels. In the absence of antibodies (Fig. 4B, lane 1), protein-coated QDs migrated towards the anode at the bottom of the gel, and there was a good match between the BB-TrxA::CT43 protein band on Coomassie-stained gels (top), and the fluorescent band when the same gels were photographed under UV illumination (bottom). By contrast, pure IgG migrated towards the cathode and was not fluorescent (lane 13).

Addition of increasing amounts of IgG to a fixed concentration of BB-TrxA::CT43-coated nanocrystals led to progressive disappearance of the fluorescent/fusion protein band corresponding to unmodified QDs, and to the concomitant appearance of two intermediate bands designated "a" and "b" in Fig. 4B. Band "a" was detected at ratios of IgG to fusion protein ranging from 1:6 to 1:1 and likely corresponds to nanocrystals that are not completely derivatized with antibodies. At a twofold molar excess of IgG over BB-TrxA::CT43, all fluorescent/fusion protein material was found at position "b" and there was no change in migration when the IgG concentration was raised up to a 6-fold molar excess. Thus, band "b" corresponds to fully-derivatized immuno-QDs in which every sterically available BB domain has bound an antibody Fc fragment as depicted in Fig. 4A. Based on atomic emission spectroscopy data and assuming that the nanocrystals are 4.1 nm diameter spheres, we calculated that 5 to 6 molecules of BB-TrxA::CT43 cap each ZnS:Mn particle. Why we were only able to visualize a single species of intermediate valency rather than a series of bands decorated with different numbers of antibodies remains unclear but may be

related to the poor resolution of agarose electrophoresis and/or cooperative binding events. Nevertheless, the equilibrium co-existence of underivatized, fully derivatized and partially derivatized QDs at low IgG concentrations indicates that it is possible to generate stable species displaying variable numbers of decorating antibodies to the solvent. Finally, it is worth pointing out that the interaction between BB-TrxA::CT43-coated QDs and IgG was robust and specific since addition of up to a 3-fold molar excess of BSA did not affect immuno-QD formation (Fig. S3).

To verify immuno-QD functionality with a different type of antibody, we conducted an antigen aggregation experiment as depicted in Fig. 5A. To this end, ZnS:Mn nanocrystals were mixed with a twofold molar excess (1 nmole) of rabbit anti-Bovine Serum Albumin (BSA) over the amount of BB-TrxA::CT43 used for their mineralization. Based on Fig. 4, these conditions should result in a protein shell that is fully decorated with polyclonal anti-BSA antibodies. Next, 50 pmoles of BSA were added to the mixture. As anticipated from the fact that the multivalent immuno-QDs recognize several epitopes on each BSA molecule, we observed the formation of micrometer size aggregates that were highly fluorescent due to the spatial confinement of a large numbers of QDs (Fig. 5B). No such clusters were observed when the experiment was repeated with nanocrystals that had not been first decorated with antibodies (Fig. S4).

In order to further demonstrate the practical usefulness of the above immunoconjugates, we fractionated decreasing amounts of hexahistidine-tagged Hsp31 (His_6-Hsp31, a molecular chaperone from *E. coli*)[21] on SDS minigels and transferred samples to PVDF membranes. The control membrane (Fig. 6A) was incubated with antibodies against the hexahistidine tag antibodies and His_6-Hsp31 bands were detected following incubation with alkaline phosphatase conjugated secondary antibodies and colorimetric development. The duplicate membrane was directly probed with QDs decorated with the same amount of anti-His_6 antibodies (in buffer containing 150 mM NaCl) and photographed on a UV transilluminator. Fig. 6B shows that immuno-QD detection was not only more rapid (single-step) but also more sensitive than colorimetry, allowing visualization of as little as 0.5 ng (≈ 15 fmol) of His_6-Hsp31.

CONCLUSION

We have developed a straightforward and environmentally friendly biomineralization process for the synthesis of multicolored ZnS nanocrystals *via* aqueous and low-temperature transition metal doping. Biofabricated ZnS:Mn QDs appear particularly promising for bioimaging and biosensing applications because: (1) they emit bright yellow-orange light upon excitation with standard UV sources, have long shelf lives and are stable under physiological conditions of pH and ionic strength; (2) their core does not incorporate cadmium ions that persist for long times in tissues;[22,23] (3) the capping protein shell is stably tethered to the crystalline through the mineralizing ZnS binding peptide and can be readily derivatized with antibodies owing to the presence of the BB domain; and (4) the antigen-binding valency of the resulting nanoparticles can be controlled by varying the molar ratio of antibodies to fusion protein.

MATERIALS AND METHODS

Materials

All chemicals were purchased from Sigma-Aldrich Co and fresh stock solutions were prepared on the day of use with Milli-Q grade ddH_2O water. The BB-TrxA::CT43 fusion protein was expressed, purified and desalted as described,[13] and was stored at −80°C. Before use, the protein was thawed and dialyzed overnight at 4°C against ddH_2O.

Nanocrystal Synthesis

For the synthesis of Mn-doped ZnS nanocrystals, we modified our original protocol[13] as follows: 200 μL of 5 mM $Zn(CH_3COO)_2$ was aliquoted in an 18 mm diameter round-bottom test tube, and appropriate amounts of 5 mM $Mn(CH_3COO)_2$ were added to change the Mn^{2+}:Zn^{2+} molar ratio from 1:200 to 1:3. Next, 200 μL of 40 mM NH_4CH_3COO and 244 μL of 0.55 mg/mL BB-TrxA::CT43 were added. The pH was adjusted to 8.2 by addition of 250 μL of 10 mM NH_4OH and the volume brought to 2.3 mL with ddH_2O. After 1h incubation at room temperature, 200μL of 5 mM Na_2S was added dropwise with vortexing and the solution was transferred to a 37°C incubator for a 5 days aging period. The final concentration of both cations (Zn^{2+} + Mn^{2+}) and anions (S^{2-}) was 0.4 mM, while the final concentration of BB-Trx::CT43 was 2 μM. Long-term nanocrystal sample storage was at 4°C. Cu-doped ZnS nanocrystals were prepared as above except that a stock solution of 5 mM $Cu(CH_3COO)_2$ was used in place of $Mn(CH_3COO)_2$.

Analytical Techniques

UV-visible absorption spectra were measured on a Beckman Coulter DU640 spectrophotometer using 1 mL of sample. Photoluminescence emission spectra were recorded from 300 to 800 nm using 1 mL of sample on a Hitachi F4500 fluorescence spectrophotometer with excitation at 280 nm and slit widths set at 2.5 nm. The wavelength region corresponding to the second order diffraction peak of the excitation light was omitted. Photoluminescence excitation spectra were collected at 590 nm (ZnS:Mn) or 480 nm (ZnS:Cu) over the indicated range of excitation wavelengths on the same instrument. Hydrodynamic diameters were measured on a Malvern Zetasizer Nano-ZS dynamic light scattering instrument equipped with a 633 nm laser filter using 1 mL samples. For transmission electron microscopy (TEM) analysis, samples (5 μL) were deposited on plasma-cleaned carbon-coated copper TEM grids and allowed to dry in air. High-resolution TEM images were collected on a FEI Tecnai G2 F20 S/TEM operated at an accelerating voltage of 200 kV. For induction coupled plasma (ICP) atomic emission spectroscopy, 10 mL of 7.5% or 10% Mn-doped ZnS QDs were mixed with 50 mL of acetone and the precipitated material was sedimented by centrifugation at 5000 g for 5 min. The pellet was washed twice with 5 mL acetone and allowed to air dry. Concentrated HCl (2.5 mL) and HNO_3 (2.5 mL) were added sequentially and the mixture was incubated for 4h. Samples were diluted 10-fold for ICP atomic emission spectroscopy on Jarrell-Ash 955. Calibration standards in the 0–50 μM (Mn2+) and 0–400 μM (Zn2+) range were prepared with $Mn(CH_3COO)_2$ or $Zn(CH_3COO)_2$ as above. All measurements were conducted in triplicate.

Native Agarose Electrophoresis

Samples of ZnS:Mn quantum dots were concentrated ≈ 4 times by centrifugation at 4,000 *g* using an Amicon Ultra-4 centrifugal filter (MWCO 3kDa, Millipore). The retentate was assayed for BB-TrxA::CT43 concentration (assumed to be quantitatively bound to the nanocrystals) using a Bradford assay (Pierce). The typical concentration of fusion protein was 0.2 mg/mL (7.5 μM). Human IgG purified immunoglobin (Sigma) was dissolved to a 10 mg/mL (66.7 μM) or 2 mg/mL (13.3 μM) concentration in buffer A (100 mM Tris-HCl, pH 7.5, 150 mM NaCl). Bovine serum albumin (BSA; Sigma) was dissolved to a concentration of 2 mg/mL (30 μM) in the same buffer. A constant amount of ZnS:Mn nanocrystals (30 μL) was mixed with various amounts of IgG to change the molar ratio of IgG to BB-TrxA::CT43 from 1:6 to 6:1 and the final volume was adjusted to 60 μL with buffer A. For the control experiment of Fig. S3, ZnS:Mn nanocrystals were mixed at equimolar ratio of IgG to BB-TrxA::CT43 in the absence or presence of the indicated molar excess of BSA. After 1h incubation at 4°C with slow shaking, immunocomplexes were mixed with 10 μL of 5× sample buffer (50% glycerol, 0.1% Bromophenol Blue, 0.12 M Tris base), and aliquots were loaded onto 0.75% agarose gels made in running buffer (25 mM Tris, 19.2 mM glycine, pH

8.5). Aliquots of the concentrated QD solution and human-IgG were loaded in flanking wells to serve as controls. The gel was submerged in running buffer and electrophoresis was performed at a constant voltage of 50 V for 45 min (or 60 min in the case of Fig. S3) at room temperature. Fluorescent bands were detected by illumination at 302 nm on a UV transilluminator operating at 302 nm. Gels were subsequently stained with 0.12% Coomassie brilliant blue R in 45% methanol and 10% acetic acid for 1 h, and destained in 45% methanol, 10% acetic acid, before digital image acquisition.

Western Blots

Aliquots of His_6-HSP31 expressed and purified as described[21] were loaded onto duplicate 12.5% SDS-PAGE minigels and transferred to PVDF membranes at 65 V for 65 min. The membranes were incubated for 1h at room temperature in a blocking solution consisting of 3% gelatin and 3% BSA in TBS-T buffer (20 mM Tris-base, pH 7.5, 500 mM NaCl, 0.05% Tween-20). For colorimetric detection, the membrane was rinsed 3 times with TBS-T and incubated for 1h at room temperature in 10 mL of blocking buffer supplemented with anti-HexaHis mouse monoclonal antibody (Covance) at a 1:1,000 dilution. After 3 wash steps in TBS-T, the membrane was incubated for 1h at room temperature in 10 mL of blocking buffer supplemented with a 1:3,000 dilution of goat anti-mouse IgG alkaline phosphatase conjugate (Sigma). Immunoreactive bands were visualized by colorimetric detection with NBT and BCIP. For QD-based detection, 2 mL of unconcentrated ZnS:Mn nanocrystals were mixed with an equal volume of blocking solution and the anti-HexaHis antibody was added at a 1:1000 dilution and the solution was incubated 1h at 4°C. The membrane was immersed in the detection reagent for 1h, washed 3 times with TBS-T and fluorescent bands were visualized by photographing the membrane on a UV transilluminator operated at 302 nm.

Antigen Aggregation Assay

Biofabricated ZnS:Mn QDs (250 μL) were incubated with 30 μL of rabbit anti-BSA (Sigma B1520; 5 mg/mL) for 1h at room temperature with gentle mixing. A 33.3 μL aliquot of a 100 Hg/mL solution of purified BSA (50 pmoles) was added and the mixture was incubated for one additional hour at room temperature. An aliquot (5 μL) was photographed on a Nikon inverted microscope with a 40x/1.3 oil objective and UV illumination from a Hg lamp. The control experiment of Fig. S4 was conducted as above but without anti-BSA addition.

Supplementary Material

Refer to Web version on PubMed Central for supplementary material.

Acknowledgments

We are grateful to Vladimir Vlaskin and Dan Gamelin for helping with ICP atomic emission spectroscopy. This work was funded by a NSF NIRT award (CMMI-0709131), the NSF-funded Genetically Engineered Materials Science and Engineering Center (DMR-0520657), and NIH-NIEHS award 1U19ES019545-01. Part of the work was conducted at the University of Washington Nanotech User Facility, a member of the NSF National Nanotechnology Infrastructure Network.

REFERENCES AND NOTES

1. Chan WCW, Nie S. Quantum Dot Bioconjugates for Ultrasensitive Nonisotopic Detection. Science. 1998; 281:2016–2018. [PubMed: 9748158]
2. Gao X, Cui Y, Levenson RM, Chung LW, Nie S. In Vivo Cancer Targeting and Imaging with Semiconductor Quantum Dots. Nat Biotechnol. 2004; 22:969–976. [PubMed: 15258594]

3. Jamieson T, Bakhshi R, Petrova D, Pocock R, Imani M, Seifalian AM. Biological Applications of Quantum Dots. Biomaterials. 2007; 28:4717–4732. [PubMed: 17686516]
4. Medintz IL, Uyeda HT, Goldman ER, Mattoussi H. Quantum Dot Bioconjugates for Imaging, Labeling and Sensing. Nat Mater. 2005; 4:435–446. [PubMed: 15928695]
5. Michalet X, Pinaud FF, Bentolila LA, Tsay JM, Doose S, Li JJ, Sundaresan G, Wu AM, Gambhir SS, Weiss S. Quantum Dots for Live Cells, In Vivo Imaging and Diagnostics. Science. 2005; 307:538–544. [PubMed: 15681376]
6. Biju V, Itoh T, Anas A, Sujith A, Ishikawa M. Semiconductor Quantum Dots and Metal Nanoparticles: Syntheses, Optical Properties and Biological Applications. Anal Bioanal Chem. 2008; 391:2469–2495. [PubMed: 18548237]
7. Dabbousi BO, Rodriguez-Viejo J, Mikulec FV, Heine JR, Mattoussi H, Ober R, Jensen KF, Bawendi MG. (CdSe)ZnS Core-Shell Quantum Dots: Synthesis and Characterization of a Size Series of Highly Luminescent Nanocrystallites. J Phys Chem B. 1997; 101:9463–9475.
8. Hines MA, Guyot-Sionnest P. Synthesis and Characterization of Strongly Luminescing ZnS-Capped CdSe Nanocrystals. J Phys Chem. 1996; 100:468–471.
9. Baneyx F, Schwartz DT. Selection and Analysis of Solid-Binding Peptides. Curr Opin Biotechnol. 2007; 18:312–317. [PubMed: 17616387]
10. Dickerson MB, Sandhage KH, Naik RR. Protein- and Peptide Directed Synthesis of Inorganic Materials. Chem Rev. 2008; 108:4935–4978. [PubMed: 18973389]
11. Sarikaya M, Tamerler C, Jen AK, Schulten K, Baneyx F. Molecular Biomimetics: Nanotechnology through Niology. Nat Mater. 2003; 2:577–585. [PubMed: 12951599]
12. Sarikaya M, Tamerler C, Schwartz DT, Baneyx F. Materials Assembly and Formation Using Engineered Polypeptides. Annu Rev Mater Res. 2004; 34:373–408.
13. Zhou W, Schwartz DT, Baneyx F. Single Pot Biofabrication of Zinc Sulfide Immuno-Quantum Dots. J Am Chem Soc. 2010; 132:4731–4738. [PubMed: 20218715]
14. Clarke S, Pinaud F, Beutel O, You C, Piehler J, Dahan M. Covalent Monofunctionalization of Peptide-Coated Quantum Dots for Single-Molecule Assays. Nano Lett. 2010; 10:2147–2154. [PubMed: 20433164]
15. Manzoor K, Johny S, Thomas D, Setua S, Menon D, Nair S. Bio-Conjugated Luminescent Quantum Dots of Doped ZnS: a Cyto-Friendly System for Targeted Cancer Imaging. Nanotechnology. 2009; 20:065102. [PubMed: 19417370]
16. Norris DJ, Efros AL, Erwin SC. Doped Nanocrystals. Science. 2008; 319:1776–1779. [PubMed: 18369131]
17. Quan Z, Wang Z, Yang P, Lin J, Fang J. Synthesis and Characterization of High-Quality ZnS, ZnS:Mn^{2+}, and ZnS:Mn^{2+}/ZnS (Core/Shell) Luminescent Nanocrystals. Inorg Chem. 2007; 46:1354–1360. [PubMed: 17243762]
18. Sooklal K, Cullum BS, Angel M, Murphy CJ. Photophysical Properties of ZnS Nanoclusters with Spatially Localized Mn^{2+} J Phys Chem. 1996; 100:4551–4555.
19. Malik MA, RO'Brien P, Revaprasadu N. Synthesis of TOPO-Capped Mn-Doped ZnS and CdS Quantum Dots. J Mater Chem. 2001; 11:2382–2386.
20. Khosravi AA, Kundu M, Jatwa L, Deshpande SK, Bhagwat UA, Sastry M, Kulkarni SK. Green Luminescence from Copper Doped Zinc Sulphide Quantum Particles. Appl Phys Lett. 1995; 67:2702–2704.
21. Sastry MSR, Quigley PM, Hol WGJ, Baneyx F. The Linker-Loop Region of *E. coli* Chaperone Hsp31 Functions as a Thermal Gate That Modulates High Affinity Substrate Binding at Elevated Temperatures. Proc Natl Acad Sci U S A. 2004; 101:8587–8592. [PubMed: 15173574]
22. Lee HA, Leavens TL, Mason SE, Monteiro-Riviere NA, Riviere JE. Comparison of Quantum Dot Biodistribution with a Blood-Flow Limited Physiologically Based Pharmacokinetic Model. Nano Lett. 2009; 9:794–799. [PubMed: 19128005]
23. Lin P, Chen JW, Chang LW, Wu JP, Redding L, Chang H, Yeh TK, Yang CS, Tsai MH, Wang HJ, et al. Computational and Ultrastructural Toxicology of a Nanoparticle, Quantum dot 705, in Mice. Environ Sci Technol. 2008; 42:6246–6270.

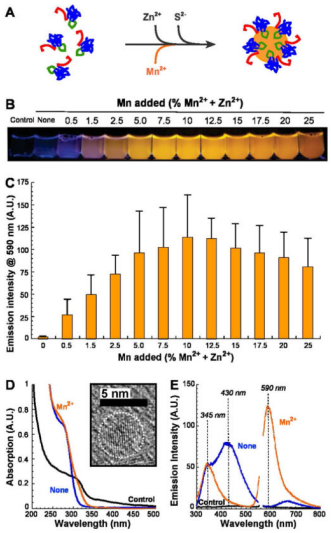

Figure 1.

Protein-aided synthesis of Mn-doped ZnS nanocrystals. (A) Schematic illustration of the biomineralization process mediated by the BB-TrxA::CT43 fusion protein. The antibody-binding BB domain (red), ZnS-binding loop (green) and TrxA framework (blue) are shown. (B) Influence of the Mn^{2+} concentration on the fluorescence of UV-excited biofabricated QDs. A no protein control is included. (C) Emission intensity at 590 nm of QDs mineralized in the presence of the indicated amount of Mn^{2+} (λ_{ex} = 280 nm). Error bars correspond to triplicate experiments. Absorption (D) and emission (E) spectra of QD mineralized in the absence (blue) or presence of 7.5% Mn (orange). A no protein control (black) is included. The peak centered at 670 nm that is visible in the blue curve and convoluted in the orange spectrum corresponds to the second order diffraction of the proteins' tryptophan emission peak. The inset of Fig. D shows a HRTEM image of an Mn-doped (7.5%) ZnS nanocrystals bounded by a dashed line to facilitate visualization.

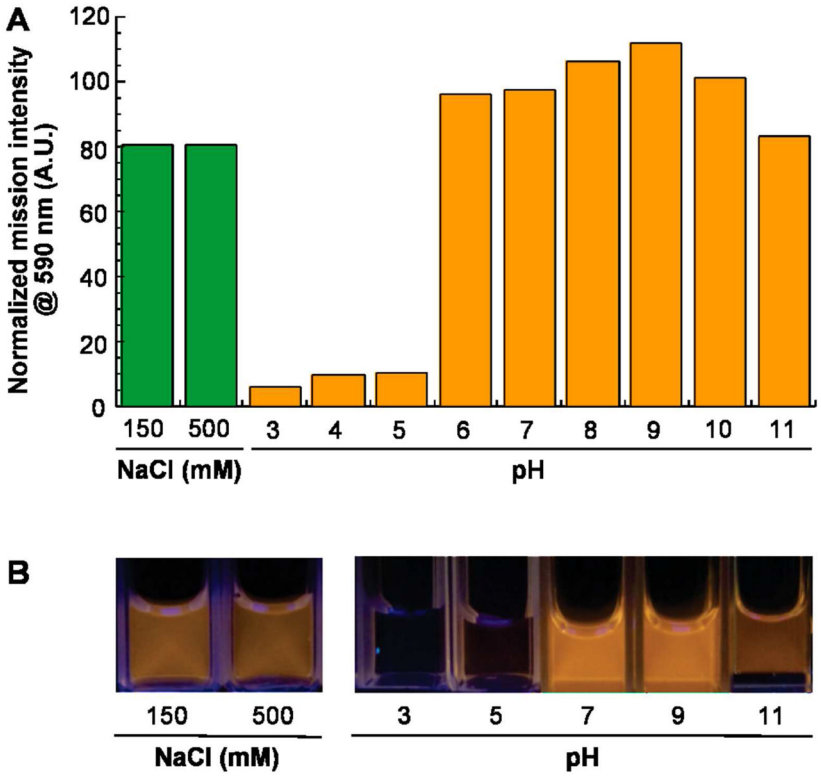

Figure 2.

Influence of ionic strength and pH on the optical performance of biofabricated ZnS:Mn QDs. (A) Photoluminescence intensities were recorded at 590 nm after 1h incubation at 23°C in the presence of the indicated additives. Values are normalized to that of an untreated control sample. There was no change in intensity after an additional hour of incubation. (B) Appearance of the samples.

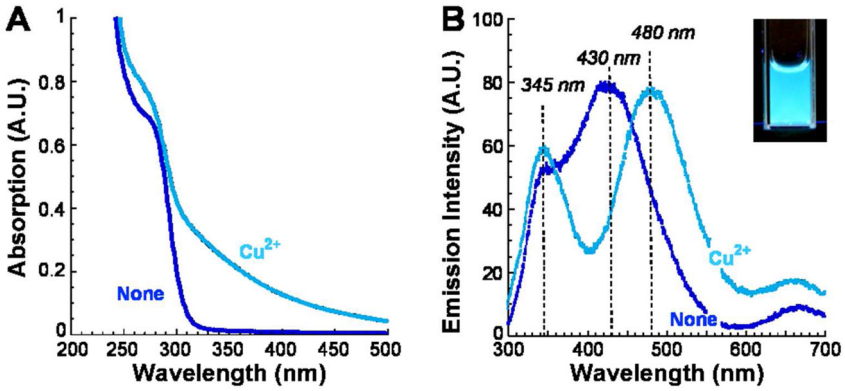

Figure 3.

Photopysical characteristics of biofabricated ZnS QDs doped with Cu(II). Absorption (A) and emission (B) spectra were collected for sample receiving no additives (None) or 2.5% Cu^{2+}. The inset shows the appearance of Cu(II)-doped (2.5%) ZnS QDs.

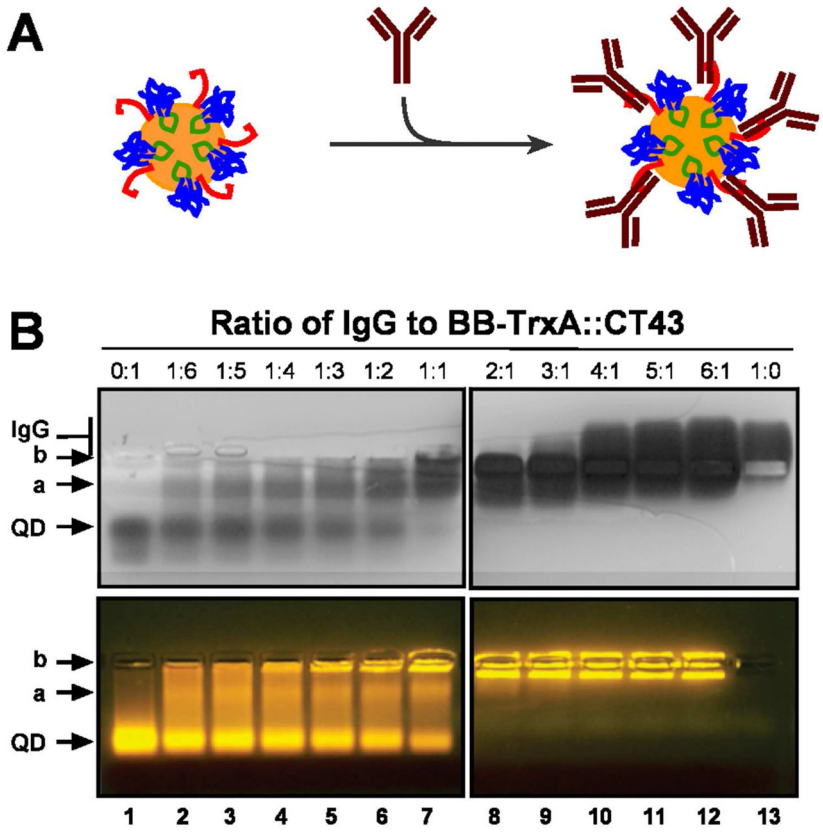

Figure 4.

Controlling the valency of immuno-QDs. (A) Schematic illustration of the antibody conjugation process through the BB domain (red) of the capping fusion protein. (B) Agarose gel analysis of immuno-complex formation at various IgG to QD ratios. The gels were stained with Coomassie blue (top images) or photographed under UV light (bottom). The migration position of unconjugated QDs and IgG are indicated, as is the position of two different immuno-conjugates (a and b).

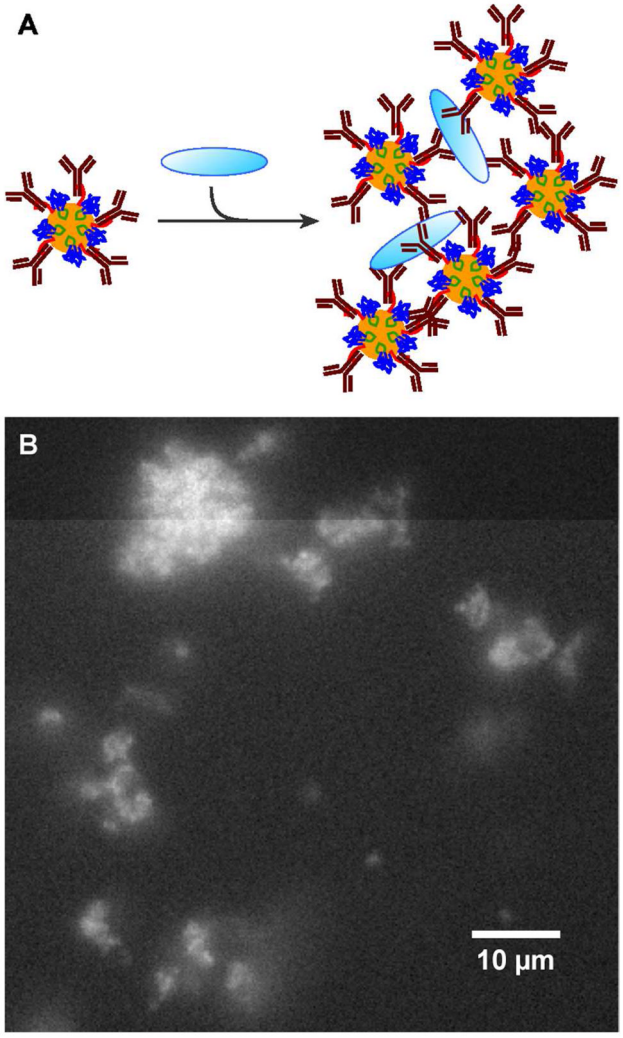

Figure 5.
Antigen aggregation assay. (A) Schematic illustration of the assay in which multiple epitopes on BSA (pale blue oval) are recognized by a molar excess of QDs decorated with anti-BSA polyclonal antibodies. (B) Fluorescence image of the resulting aggregates.

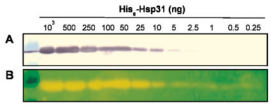

Figure 6.
Western analysis of His6-Hsp31 using anti-histidine antibodies and traditional (A) or ZnS:Mn QD-based (B) detection.